GEORG-AUGUST-UNIVERSITÄT GÖTTINGEN

Fakultät für Physik

Bachelor's Thesis

Hier steht das Thema der Arbeit in deutsch

Here comes the title of the thesis in english

prepared by

Timo Janßen

from Westerstede

at the Institut für heftige Physik

Thesis period: 1. Januar 2000 until 1. Januar 2000

Supervisor: Dr. X

First referee: Prof. Dr. X

Second referee: Prof. Dr. Newton

Kurzfassung

<insert your name>

<insert title>

Schlagwörter: <insert key words>

Abstract

<insert your name>

<insert title (english)>

Key words: <insert key words>

Inhaltsverzeichnis

KAPITEL 1

Einleitung

KAPITEL 2

Grundlagen

2.1 Next-to-leading order calculations

…(need real and virtual, both seperately divergent, need to regularize)

There are two general methods that are commonly used to take care of the infrared deivergences in NLO calculations, namely the *slicing method* and the *subtraction method*. We can demonstrate both methods with a simple example similar to the depiction in [20]. Consider the integral

$$I = \lim_{\epsilon \to 0} \left(\int_0^1 \frac{\mathrm{d}x}{x} x^\epsilon F(x) - \frac{1}{\epsilon} F(0) \right) , \tag{2.1}$$

where $F(x)$ is an arbitrary function that depends on x. The first term contains a singularity at $x = 0$ and is divergent in the limit $\epsilon \to 0$. This divergence is canceled by the second term. The parameter ϵ can be compared to the parameter used in dimensional regularization. As a consequence of $F(x)$ being arbitrary complex, the integral can not be solved analytically. However, in this form it is also not well-suited for a numerical evalution because of the presence of ϵ in the integrand.

In the slicing method, one introduces a small parameter δ, which slices the integration region into two pieces, so that the integral can be written in the following way:

$$
\begin{aligned}
I &= \lim_{\epsilon\to 0}\left(\int_0^\delta \frac{\mathrm{d}x}{x}x^\epsilon F(x) + \int_\delta^1 \frac{\mathrm{d}x}{x}x^\epsilon F(x) - \frac{1}{\epsilon}F(0)\right) \\
&= \lim_{\epsilon\to 0}\left(F(0)\int_0^\delta \frac{\mathrm{d}x}{x}x^\epsilon - \frac{1}{\epsilon}F(0)\right) + \int_\delta^1 \frac{\mathrm{d}x}{x}F(x) + \mathcal{O}(\delta) \\
&= F(0)\lim_{\epsilon\to 0}\frac{\delta^\epsilon - 1}{\epsilon} + \int_\delta^1 \frac{\mathrm{d}x}{x}F(x) + \mathcal{O}(\delta) \\
&= F(0)\ln\delta + \int_\delta^1 \frac{\mathrm{d}x}{x}F(x) + \mathcal{O}(\delta)\,.
\end{aligned}
\tag{2.2}
$$

Therefore, the dependence on ϵ has vanished completely and the remaining integral can be computed numerically. The terms $\mathcal{O}(\delta)$ are neglectable if δ is small. In an actual calculation, one would have to check that the result does not depend on the choice of δ.

The subtraction method does not involve any approximations. Instead, one rewrites the integral in the form

$$
\begin{aligned}
I &= \lim_{\epsilon\to 0}\left(\int_0^1 \frac{\mathrm{d}x}{x}x^\epsilon[F(x) - F(0)] + F(0)\int_0^1 \frac{\mathrm{d}x}{x}x^\epsilon - \frac{1}{\epsilon}F(0)\right) \\
&= \int_0^1 \frac{\mathrm{d}x}{x}[F(x) - F(0)]\,,
\end{aligned}
\tag{2.3}
$$

which automatically leads to a form that can be evaluated by a numerical integration algorithm. We can take a look at how this method works in a somewhat more realistic calculation. Consider the expression for the expectation value of an infrared-safe observable O at NLO accuracy, consisting of a Born (B), a virtual (V) und a real (R) term:

$$
\langle O\rangle = \lim_{\epsilon\to 0}\int_0^1 \mathrm{d}x x^{-2\epsilon} O(x)\left[\left(\tfrac{\mathrm{d}\sigma}{\mathrm{d}x}\right)_B + \left(\tfrac{\mathrm{d}\sigma}{\mathrm{d}x}\right)_V + \left(\tfrac{\mathrm{d}\sigma}{\mathrm{d}x}\right)_R\right]\,. \tag{2.4}
$$

We assume that the cross sections can be written as

$$\left(\frac{\mathrm{d}\sigma}{\mathrm{d}x}\right)_B = B\delta(x)\,, \tag{2.5}$$

$$\left(\frac{\mathrm{d}\sigma}{\mathrm{d}x}\right)_V = a\left(\frac{B}{2\epsilon}+V\right)\delta(x)\,, \tag{2.6}$$

$$\left(\frac{\mathrm{d}\sigma}{\mathrm{d}x}\right)_R = a\frac{R(x)}{x} \tag{2.7}$$

where B and V are constant factors and $\lim_{x\to 0} R(x) = B$. a denotes the coupling constant. This model has been adapted from [15]. Obviously, both the real and the virtual part are divergent in the limit $\epsilon \to 0$. Using the subtraction method analogous to the case above, we can rewrite the real contribution to obtain

$$\begin{aligned}\langle O\rangle_R &= a\lim_{\epsilon\to 0}\int_0^1 \frac{\mathrm{d}x}{x^{1+2\epsilon}}O(x)R(x)\\ &= aBO(0)\lim_{\epsilon\to 0}\int_0^1 \frac{\mathrm{d}x}{x^{1+2\epsilon}} + a\int_0^1 \frac{\mathrm{d}x}{x}[O(x)R(x)-BO(0)]\\ &= -aBO(0)\lim_{\epsilon\to 0}\frac{1}{2\epsilon} + a\int_0^1 \frac{\mathrm{d}x}{x}[O(x)R(x)-BO(0)]\,. \end{aligned} \tag{2.8}$$

By explicitely writing down the virtual part,

$$\langle o\rangle_V = a\lim_{\epsilon\to 0}\int_0^1 \frac{\mathrm{d}x}{x^{2\epsilon}}O(x)\left(\frac{B}{2\epsilon}+V\right)\delta(x)\,, \tag{2.9}$$

we see that the first term gets exactly cancelled by the first term on the right hand side of (2.8). Including the Born contribtion we arrive at the expression

$$\langle O\rangle = BO(0) + a\left\{VO(0) + \int_0^1 \frac{\mathrm{d}x}{x}[O(x)R(x)-BO(0)]\right\}\,. \tag{2.10}$$

It now consists of three terms that are separately finite: The leading order Born term (B), the integrated virtual term (VI) and the real subtracted term (RS).

2.2 Reweighting QCD calculations

Often it is needed to vary the parameters in QCD calculations, for example the scale variables and PDFs to estimate the uncertainty. When the number of variations becomes large, it is not practical to rerun the whole event generation for each calculation as the time and resource consumption become too high. Instead it is possible to reuse information from previously generated events and combine them with the new parameters. For a leading order calculation, this is straightforward: Consider the leading order parton model cross section for producing an arbitrary final state X:

$$\sigma_{pp\to X} = \sum_{i,j} \int \mathrm{d}x_1\, \mathrm{d}x_2 \int \mathrm{d}\Phi_n \left(\frac{\alpha_s(\mu_R^2)}{2\pi}\right)^{p_{\mathrm{LO}}} \mathrm{f}_i(x_1, \mu_F^2)\, \mathrm{f}_j(x_2, \mu_F^2)\, \mathrm{d}\hat{\sigma}_{ij\to X}\,. \tag{2.11}$$

The squared matrix element for the parton-level subprocess $2 \to n$ is denoted by $\mathrm{d}\hat{\sigma}_{ij\to X}$, differential in the phase space $\mathrm{d}\Phi_n$. We can group subprocesses s with the same parton-level cross section into a cumulated parton density $\mathrm{F}_s(x_1, x_2, \mu_F^2)$ and write

$$\sigma_{pp\to X} = \int \mathrm{d}x_1\, \mathrm{d}x_2 \int \mathrm{d}\Phi_n \left(\frac{\alpha_s(\mu_R^2)}{2\pi}\right)^{p_{\mathrm{LO}}} \mathrm{F}_s(x_1, x_2, \mu_F^2)\, \mathrm{d}\hat{\sigma}_{ij\to X}\,. \tag{2.12}$$

Rewriting this in a form that can be computed by a Monte Carlo algorithm on a per-event basis, we arrive at

$$\sigma_{pp\to X} = \sum_{e=1}^{N_{\mathrm{evt}}} \left(\frac{\alpha_s(\mu_R^2)}{2\pi}\right)^{p_{\mathrm{LO}}} w_e(k_e)\, \mathrm{F}_{s_e}(x_1, x_2, \mu_F^2)\,. \tag{2.13}$$

The event weight $w_e(k_e)$ is given by

$$w_e(k_e) = \Pi_{\mathrm{ps}}(k_e)\Theta(k_e - k_{\mathrm{cuts}})\, \mathrm{d}\hat{\sigma}_e \tag{2.14}$$

and represents the subprocess cross section $d\hat{\sigma}_e$ with respect to the phase space weight $\Pi_{\text{ps}}(k_e)$ and the kinematic cuts. The kinematic parameters for each event are combined in

$$k_e = \{p_1, \dots, p_n, x_1, x_2\} \ , \tag{2.15}$$

where the p_i denote the involved partons.

Provided that all event weights have been stored, using a diferent PDF is as simple as multplying each weight with the new PDF $\mathrm{F}^{\text{new}}_{s_e}(x_1, x_2, \mu_F^2)$. The value of α_s can be changed similarly. To vary the scales, only α_s and F_{s_e} have to be reevaluated as the weights themselves do not depend on the scales.

2.3 The considered process: Higgs production through gluon fusion

In this thesis, the considered process will be the production of a Higgs boson through gluon fusion. Although there are other possible production mechanisms in the Standard Model, this is the main process at the LHC, with an expected cross section of $\approx 50\,\text{pb}$ at a center-of-mass energy of $\sqrt{s} = 14\,\text{TeV}$ and a Higgs mass of $125\,\text{GeV}$. [10] It proceeds through a triangular loop of heavy quarks (mainly top quarks as the Higgs coupling scales with the quark mass) as is shown in Figure 2.1

In the narrow-width approximation, the leading order cross section is given by [16]

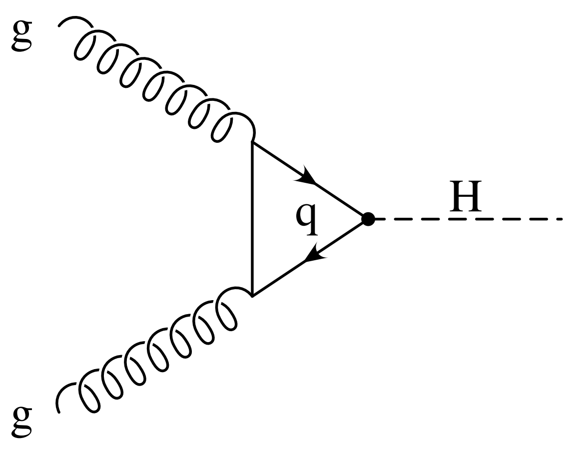

Abbildung 2.1: Higgs production through gluon fusion.

$$\sigma_{\text{LO}}(pp \to H) = \sigma_0^H \tau_H \tfrac{\mathrm{d}\,\mathcal{L}^{gg}}{\mathrm{d}\tau_H}\,, \tag{2.16}$$

where $\tau_H = M_H^2/s$ is the Drell-Yan variable and $\mathrm{d}\mathcal{L}^{gg}\,/\,\mathrm{d}\tau_H$ is the gluon luminosity. The partonic cross section σ_0^H can be written as

$$\sigma_0^H = \frac{G_F \alpha_s^2(\mu_R^2)}{288\sqrt{2}\pi} \left| \sum_q \frac{3}{2\tau_q} \left[1 + \left(1 - \frac{1}{\tau_q} \right) f(\tau_q) \right] \right|^2 , \tag{2.17}$$

with the form factor

$$f(\tau_q) = \begin{cases} \arcsin^2\left(\sqrt{\tau_q}\right), & \tau_q < 1, \\ -\frac{1}{4}\left[\ln \frac{1+\sqrt{1-\tau_q^{-1}}}{1-\sqrt{1-\tau_q^{-1}}} - i\pi\right]^2, & \tau_q > 1, \end{cases}$$

where G_F denotes the Fermi coupling constant and $\tau_q = m_H^2/4m_q^2$. The gluon luminosity takes the form

$$\tfrac{\mathrm{d}\,\mathcal{L}^{gg}}{\mathrm{d}\tau_H} = \int_0^1 \mathrm{d}x_1\,\mathrm{d}x_2\,\mathrm{g}(x_1,\mu_F^2)\,\mathrm{g}(x_2,\mu_F^2)\delta(x_1x_2 - \tau_q) \tag{2.18}$$

with $\mathrm{g}(x,\mu_F^2)$ denoting the gluon PDF.

The QCD corrections are composed of virtual corrections to the vertices and propagators, real gluon radiation in the initial state and the contributions of the subprocesses $gq \to Hq$ and $q\bar{q} \to Hg$. Exemplary diagrams for the corrections are shown in Figure 2.2.

The NLO QCD corrections to the cross section have been calculated in [17]. They increase the cross section by a factor of 1,5 to 1,7. In the limit where the top quark has infinite mass, $m_t \to \infty$, the form factor takes the value $\frac{4}{3}$. This allows for an analytical expression for the corrections [12], which is very well suited for numerical calculations. It can be considered as an extension of the Standard Model, where the Higgs boson couples directly to gluons (effective Higgs coupling). In many cases, this

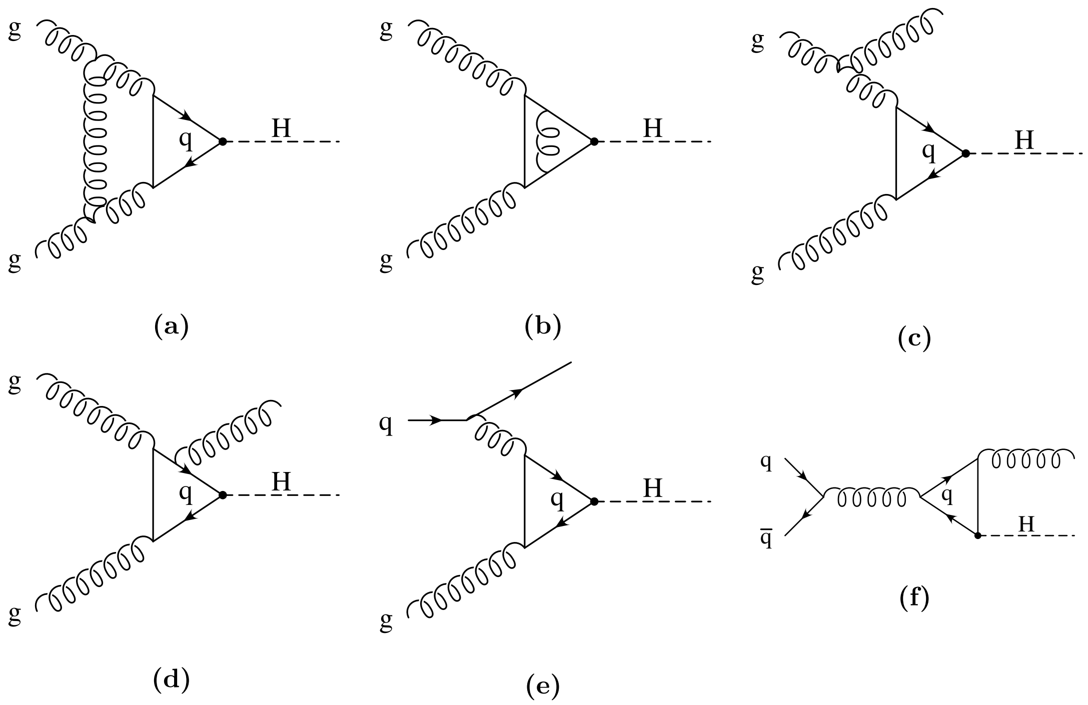

Abbildung 2.2: Example diagrams illustrating the QCD corrections to the process $pp \to H$: (a), (b) virtual corrections; (c), (d) real emission of a gluon; (e) $gq \to Hq$; (f) $q\bar{q} \to Hg$.

is a rather good approximation [13].

The NNLO corrections have been calculated in [2, 18].

A fully differential NNLO calculation exists for $H + 0 -$ jet production [3, 5] and substantial progress has been achieved towards an NNLO calculation of the $1 -$ jet cross section [7]. The fully differential NLO cross section is available for $H + 1 -$ jet [14, 21], $H + 2 -$ jets [4, 9] and $H + 3 -$ jets [8].

The effective Lagrangian for Higgs gluon interaction can be written as [2]

$$\mathcal{L}_{\text{eff}}^{ggH} = -\frac{1}{4v} C_1 G^a_{\mu\nu} G^{a\,\mu\nu} H \,, \tag{2.19}$$

where v is the Higgs vacuum expectation value, $G^a_{\mu\nu}$ is the gluon field strength tensor and H is the Higgs field. The coefficient C_1, in the $\overline{\text{MS}}$ scheme, is given by

$$C_1 = \frac{-1}{3\pi}\left\{1 + \frac{11\alpha_s}{4\pi} + \left(\frac{\alpha_s}{\pi}\right)^2\left[\frac{2777}{288} + \frac{19}{16}\log\left(\frac{\mu^2}{m_t^2}\right)\right.\right.$$
$$\left.\left. + n_f\left(-\frac{67}{96} + \frac{1}{3}\log\left(\frac{\mu^2}{m_t^2}\right)\right)\right] + \mathcal{O}(\alpha_s^3)\right\}\,, \tag{2.20}$$

where the number of active flavors should be set to $n_f = 5$. According to [2], at LO this approximation is accurate within $5\,\%$ for $m_H \approx 150\,\text{GeV}$ (which is close to the measured value $m_H \approx 126\,\text{GeV}$) and improves at NLO.

2.4 Leptonic Higgs decay

There are several possible decay channels for the Higgs boson. One has to keep in mind that the Higgs coupling is proportional to the particle masses, so that it will decay into the heaviest possible particles. Assuming a Higgs mass of $m_H = 126\,\text{GeV}$, the most relevant decay products are $q\bar{q}$ (where q denotes a bottom or charm quark), WW, ZZ, $Z\gamma$, $\gamma\gamma$, gg and $\tau^+\tau^-$ [11]. The decay into photons or gluons is only possible through intermediate loops.

The studies leading to the discovery of the Higgs boson at the LHC relied primarily on the decay modes $H \to \gamma\gamma$, $H \to ZZ$ and $H \to WW$.

...For the purpose of this thesis, we will consider the decay $H \to \tau^+\tau^-$, which has a branching ratio of approximately $6\,\%$ [19]. ...There have been searches for $H \to \tau\tau$ events in the LHC data and both ATLAS [1] and CMS [6] have published evidences for this type of decay.

KAPITEL 3

Experimentelle Vorgehensweise

3.1 ???

`APPLGRID` and `fastNLO` do not use the momentum fraction x and the factorization scale Q^2 directly in their grids. Instead they provide transformations that are supposed to achieve better coverage of the values. In the following we will concentrate on the x distribution, which is more crucial to the number of grid points needed. The functions provided by `APPLGRID` are:

$$f_0(x) = \log(\frac{1}{x} - 1) \tag{3.1}$$

$$f_1(x) = -\log(x) \tag{3.2}$$

$$f_2(x) = \sqrt{-\log(x)} \tag{3.3}$$

$$f_3(x) = -\log(x) + 5 \cdot (1 - x)\,. \tag{3.4}$$

`fastNLO` only provides the functions $f_1(x)$ and $f_2(x)$. To be used in a grid, the functions are divided into equal-sized bins. In order to avoid empty bins, the limit values are determined in a seperate „phasespace run“ before the actual fill run.

The functions (normalized to the domain $[0, 1]$ for comparability) are shown in Figure 3.1. All transformations increase the point density in the low x region, where most events should fall into. Compared against f_0, the other functions also accomplish a higher point density in the high x region. Some observables in specific processes might benefit from this.

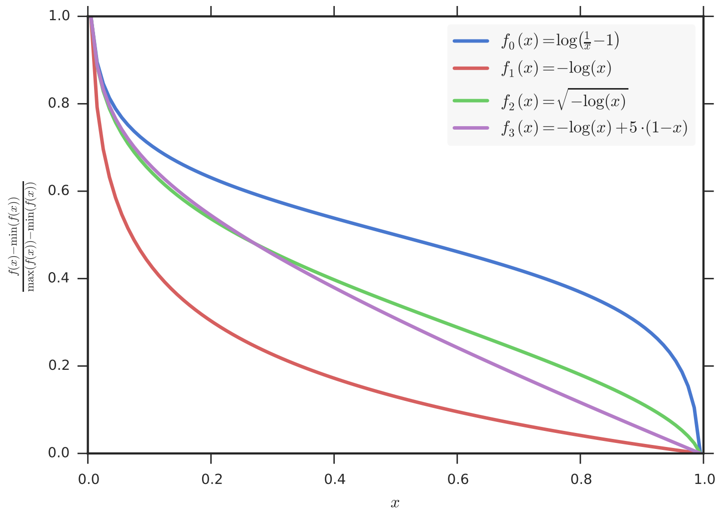

Abbildung 3.1: The transformations applied to the x distribution, normalized to the range $[0, 1]$.

We can look at the actual x distribution in the process considered in this thesis. In Figure 3.2 it is plotted for one of the gluons involved in the process $gg \to H + j$ at leading order for a center-of-mass energy of $\sqrt{s} = 13\,\text{TeV}$. For comparison, the respective distribution for the functions f_1 to f_4 is also shown. In the bare distribution, the number of events per bin increases rapidly towards low x. It is obvious that the reproduction of the low x region is poor for this linear binning. We expect that for some $x > 0$ the number of events approaches zero, because there has to be at least enough momentum transfer to produce the Higgs boson and the jet. To see this with linear binning, one would need a huge amount of bins. In contrast, the transformations are able to project the low x peak to a higher number of bins than the naive linear binning. Additionally, they all approach zero for a finite value (note that high values of $f(x)$ correspond to low values of x). Due to the normalization, this happens at 1. For all transformed distributions, it should be possible to interpolate them with a reasonable number of sampling points. The function $f_1(x)$ looks most promising, as it allocates many bins for the peak region, which should be the most relevant for this process.

If we want to be more specific, we can extract the dependence of the observables

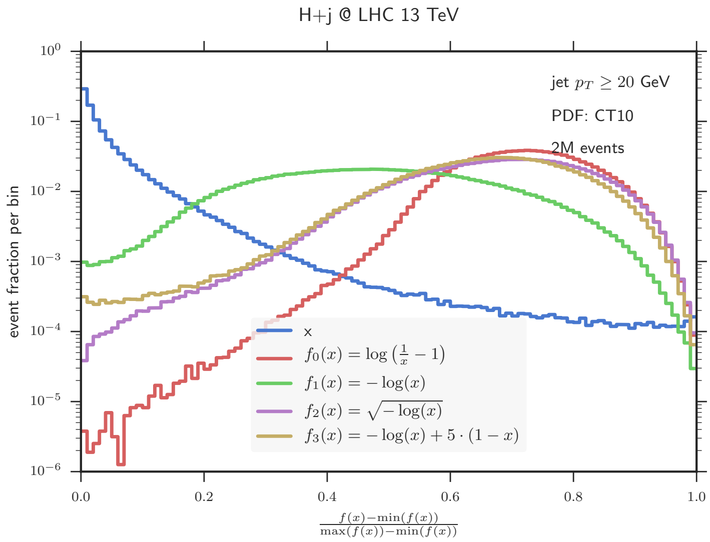

Abbildung 3.2: The event fraction per bin for the different transformations.

on x and $f(x)$, respectively, from the generated events. This is shown in Figure 3.3 for the transverse momentum $p_\perp$ and in Figure 3.4 for the rapidity y of the Higgs boson. For both observables all considered functions are reasonable. Again, the function $f_1(x)$ seems to be best suited. Hence, it will be the transformation used in all following grid calculations.

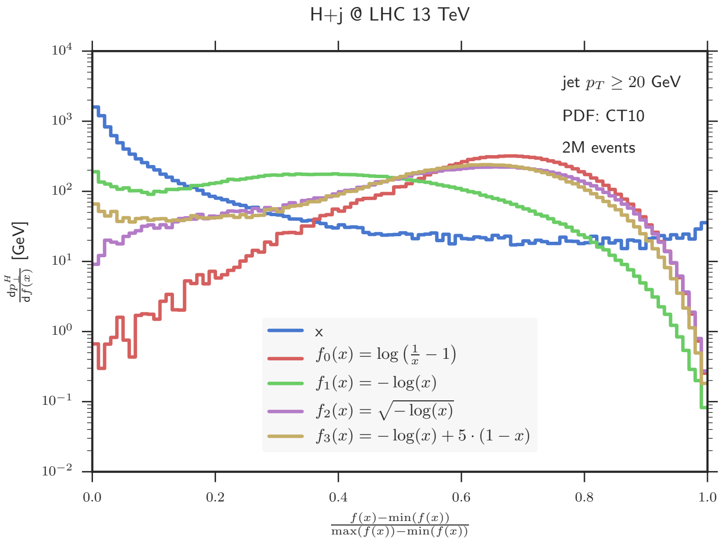

Abbildung 3.3: The transverse momentum $p_\perp$ of the Higgs boson differential in the momentum fraction x of one of the gluons.

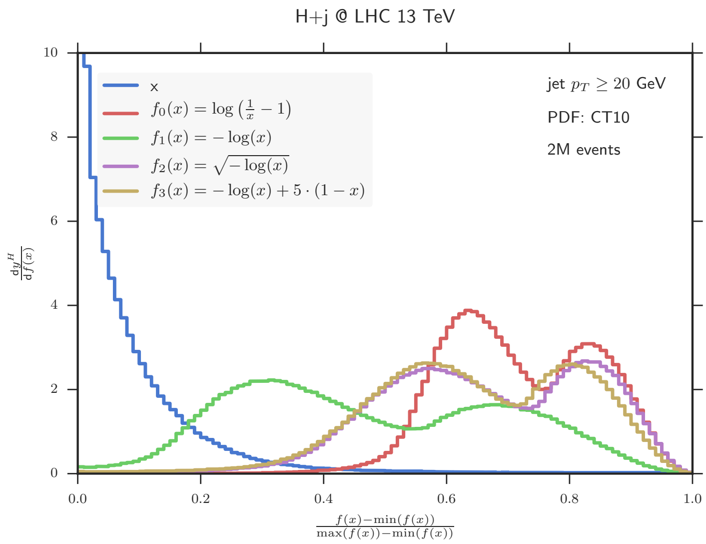

Abbildung 3.4: The rapidity y of the Higgs boson differential in the momentum fraction x of one of the gluons.

KAPITEL 4

Ergebnisse

KAPITEL 5

Diskussion

Abbildungsverzeichnis

Tabellenverzeichnis

Listings

Literatur

1. Aad, Georges u. a.: „Evidence for the Higgs-boson Yukawa coupling to tau leptons with the ATLAS detector“. *JHEP* (2015), Bd. 1504: S. 117 (siehe S. 10).
2. Anastasiou, Charalampos und Kirill Melnikov: „Higgs boson production at hadron colliders in NNLO QCD“. *Nucl.Phys.* (2002), Bd. B646: S. 220–256 (siehe S. 9, 10).
3. Anastasiou, Charalampos, Kirill Melnikov und Frank Petriello: „Fully differential Higgs boson production and the di-photon signal through next-to-next-to-leading order“. *Nucl.Phys.* (2005), Bd. B724: S. 197–246 (siehe S. 9).
4. Campbell, John M., R. Keith Ellis und Ciaran Williams: „Hadronic production of a Higgs boson and two jets at next-to-leading order“. *Phys.Rev.* (2010), Bd. D81: S. 074023 (siehe S. 9).
5. Catani, Stefano und Massimiliano Grazzini: „An NNLO subtraction formalism in hadron collisions and its application to Higgs boson production at the LHC“. *Phys.Rev.Lett.* (2007), Bd. 98: S. 222002 (siehe S. 9).
6. Chatrchyan, Serguei u. a.: „Evidence for the 125 GeV Higgs boson decaying to a pair of τ leptons“. *JHEP* (2014), Bd. 1405: S. 104 (siehe S. 10).
7. Chen, X., T. Gehrmann, E.W.N. Glover und M. Jaquier: „Precise QCD predictions for the production of Higgs + jet final states“. *Phys.Lett.* (2015), Bd. B740: S. 147–150 (siehe S. 9).

8. Cullen, G., H. van Deurzen, N. Greiner, G. Luisoni, P. Mastrolia u. a.: „Next-to-Leading-Order QCD Corrections to Higgs Boson Production Plus Three Jets in Gluon Fusion“. *Phys.Rev.Lett.* (2013), Bd. 111(13): S. 131801 (siehe S. 9).

9. Deurzen, H. van, N. Greiner, G. Luisoni, P. Mastrolia, E. Mirabella u. a.: „NLO QCD corrections to the production of Higgs plus two jets at the LHC“. *Phys.Lett.* (2013), Bd. B721: S. 74–81 (siehe S. 9).

10. Dittmaier, S. u. a.: „Handbook of LHC Higgs Cross Sections: 1. Inclusive Observables“. (2011), Bd. (siehe S. 7).

11. Dittmaier, S., S. Dittmaier, C. Mariotti, G. Passarino, R. Tanaka u. a.: „Handbook of LHC Higgs Cross Sections: 2. Differential Distributions“. (2012), Bd. (siehe S. 10).

12. Djouadi, A., M. Spira und P.M. Zerwas: „Production of Higgs bosons in proton colliders. {QCD} corrections“. *Physics Letters B* (1991), Bd. 264(3–4): S. 440–446 (siehe S. 8).

13. Djouadi, Abdelhak: „The Anatomy of electro-weak symmetry breaking. I: The Higgs boson in the standard model“. *Phys.Rept.* (2008), Bd. 457: S. 1–216 (siehe S. 9).

14. Florian, D. de, M. Grazzini und Z. Kunszt: „Higgs production with large transverse momentum in hadronic collisions at next-to-leading order“. *Phys.Rev.Lett.* (1999), Bd. 82: S. 5209–5212 (siehe S. 9).

15. Frixione, Stefano und Bryan R. Webber: „Matching NLO QCD computations and parton shower simulations“. *JHEP* (2002), Bd. 0206: S. 029 (siehe S. 5).

16. Georgi, H. M., S. L. Glashow, M. E. Machacek und D. V. Nanopoulos: „Higgs Bosons from Two-Gluon Annihilation in Proton-Proton Collisions“. *Phys. Rev. Lett.* (11 März 1978), Bd. 40: S. 692–694 (siehe S. 7).

17. Graudenz, D., M. Spira und P. M. Zerwas: „QCD corrections to Higgs-boson production at proton-proton colliders“. *Phys. Rev. Lett.* (10 März 1993), Bd. 70: S. 1372–1375 (siehe S. 8).

18. Harlander, Robert V. und William B. Kilgore: „Next-to-Next-to-Leading Order Higgs Production at Hadron Colliders“. *Phys. Rev. Lett.* (20 Mai 2002), Bd. 88: S. 201801 (siehe S. 9).

19. Heinemeyer, S u. a.: „Handbook of LHC Higgs Cross Sections: 3. Higgs Properties“. (2013), Bd. Hrsg. von Heinemeyer, S (siehe S. 10).

20. Kunszt, Zoltan und Davison E. Soper: „Calculation of jet cross sections in hadron collisions at order α_s^3“. *Phys. Rev. D* (1 Juli 1992), Bd. 46: S. 192–221 (siehe S. 3).

21. Ravindran, V., J. Smith und W.L. Van Neerven: „Next-to-leading order QCD corrections to differential distributions of Higgs boson production in hadron hadron collisions“. *Nucl.Phys.* (2002), Bd. B634: S. 247–290 (siehe S. 9).

Danksagung

Erklärung nach §13(8) der Prüfungsordnung für den Bachelor-Studiengang Physik und den Master-Studiengang Physik an der Universität Göttingen:

Hiermit erkläre ich, dass ich diese Abschlussarbeit selbständig verfasst habe, keine anderen als die angegebenen Quellen und Hilfsmittel benutzt habe und alle Stellen, die wörtlich oder sinngemäß aus veröffentlichten Schriften entnommen wurden, als solche kenntlich gemacht habe.
Darüberhinaus erkläre ich, dass diese Abschlussarbeit nicht, auch nicht auszugsweise, im Rahmen einer nichtbestandenen Prüfung an dieser oder einer anderen Hochschule eingereicht wurde.

Göttingen, den 4. Juli 2015

(Timo Janßen)

Liste der noch zu erledigenden Punkte